

Comparison between the diffusion properties of different small-scale fractional transport models

Paolo Cifani¹ and Franco Flandoli¹

¹Scuola Normale Superiore, Piazza dei Cavalieri, 7, Pisa, Italy

June 11, 2025

Abstract

Stochastic transport due to a velocity field modeled by the superposition of small-scale divergence free vector fields activated by Fractional Gaussian Noises (FGN) is numerically investigated. We present two non-trivial contributions: the first one is the definition of a model where different space-time structures can be compared on the same ground: this is achieved by imposing the same average kinetic energy to a standard Ornstein-Uhlenbeck approximation, then taking the limit to the idealized white noise structure. The second contribution, based on the previous one, is the discover that a mixing spatial structure with persistent FGN in the Fourier components induces a classical Brownian diffusion of passive particles, with suitable diffusion coefficient; namely, the memory of FGN is lost in the space complexity of the velocity field.

Keywords: Fractional Brownian Motion, Stochastic Transport, Stochastic Fluid Particles, Ornstein-Uhlenbeck, Hurst Exponent

1 Introduction

Many phenomena in nature, most prominently the motion of particles suspended in a quiescent medium, are well described by standard Brownian Motion B_t . It is often found that the physics of these problems is statistically stationary. The prototypical model for such phenomena is the Ornstein-Uhlenbeck (OU) process

$$dZ_t^\tau = -\frac{1}{\tau}Z_t^\tau dt + \left(\frac{2\sigma^2}{\tau}\right)^{1/2} dB_t \quad (1)$$

with integral timescale τ and stationary variance σ^2 . The increments dB_t are Gaussian white noise, thus samples of the latter at different times are

independent. While this is a good approximation in several instances, studies on random processes, e.g. turbulent flows and financial time series, have shown strong interdependence between distant samples. To this aim, an extension to (1) was put forward in the seminal paper [1] where long-range dependence is regulated by the Hurst exponent $H \in]0, 1[$. We can speak then of fractional Ornstein-Uhlenbeck process

$$dZ_t^{\tau, H} = -\frac{1}{\tau} Z_t^{\tau, H} dt + \frac{c_H}{\tau^H} dB_t^H \quad (2)$$

where the driving random process B_t^H is a fractional Gaussian Process of Hurst exponent H . Despite its early appearance about half a century ago, the literature on this subject is relatively young, primarily due to the difficulties, both analytically and numerically, introduced by statistical dependence of increments. Here, by means of theoretical and numerical tools, we attempt to take a step forward into the understanding of the fate of particles transported by vector fields whose components are Fractional Gaussian Processes. In particular, we will focus on stochastic transport for $H > 1/2$, i.e. positively correlated increments, and compare the findings to the case $H = 1/2$, i.e. standard Brownian Motion.

For a rigorous definition of Fractional Brownian Motion and stochastic integration in the case $H \geq 1/2$ (Young's integral) and its link with Stratonovich integration, we refer the reader to [2] (also [3], or [4]). Fractional Gaussian Processes in applications, such as turbulent fluid models, have been introduced in several works. In most cases the fractality is however understood with respect to the space-structure (see for instance [5], [6]), because of its great interest in connection with Kolmogor theory and variants like the multifractal model. The interest of Fractional Brownian Motion in time for turbulence modeling is discussed for instance in [7], see also references therein. Several very interesting works prove a fractional structure of the limit process of an homogenization procedure, rescaling of deterministic or stochastic fields; the space structure is never "chaotic" in the sense of the present paper, hence the emergence of a fractional behaviour in the limit; see for instance [8], [9], [10].

The phenomenon considered here seems to be new: we found the emergence of a Brownian behaviour in time from a space-time structure consisting of Fractional Brownian Motions in time and spatial high frequency fluctuations in all directions, which restore some independence of increments. The model considered here is similar to the one theoretically investigated in [4], where closed forms of moments of solution are found. However the case of non commuting vector fields - precisely the case which restores a degree of independence of increments - has not been theoretically solved there, only preliminary discussed, and indeed the result of the present paper is a confirmation of the fact that the time behavior is not trivial, in the non-commutative case. The model of [4] has some similarity with the model

considered in [11], where however only two Fractional Brownian Motions act, hence the restoring of independence is not possible. See also [12] for a model with some similar features.

The model considered here and in [4] is an extension to Fractional Brownian Motions of the models considered in several works in the case of classical Brownian Motion, see for instance [13], [14], [15] among several works also cited there. These papers deal with stochastic transport in Stratonovich form, a basic modeling idea performed recently for several models, also for small-scale transport of large scales - not only for transport of a passive scalars - see for instance [16], [17], [18], [19], [20], [21], [22], [23]; see also [24] for a review of diffusion limits.

The structure of this paper is organised as follows: in Sec. 2 the analytical framework is presented and the derivation of the our stochastic model is given. Specific examples of the model are then illustrated and a statement of the main claim of this work is provided. In Sec. 3 the numerical results are presented and compared with the theoretical predictions. Finally, in Sec. 4 conclusions and outlook are summarised. The analytical derivations are collected in the Appendix to facilitate the readability of this paper.

2 Stochastic transport structure

Consider the transport equation

$$\begin{aligned} \partial_t T + \mathbf{u} \cdot \nabla T &= 0 \\ T|_{t=0} &= T_0 \end{aligned} \tag{3}$$

in \mathbb{R}^2 , where $\mathbf{u}(\mathbf{x}, t)$ is a divergence free vector field. Assume that $T_0 \geq 0$ is integrable, or more conventionally that it is a probability density function (pdf), so that $T(\cdot, t)$ is also a pdf for every $t \geq 0$ (since \mathbf{u} will have the necessary regularity for such a result).

We assume that $\mathbf{u}(\mathbf{x}, t)$ is not the true solution of a fluid dynamic equation but it is a stochastic model preserving some idealized properties of a turbulent fluid, precisely a model of the following simplified form

$$\mathbf{u}(\mathbf{x}, t) = uC(\eta, \tau, H) \sum_{\mathbf{k} \in \mathbf{K}_\eta} \sigma_{\mathbf{k}}(\mathbf{x}) \frac{dB_t^{H, \mathbf{k}}}{dt} \tag{4}$$

where $C(\eta, \tau, H)$ is a normalizing constant allowing us to compare models with different space-time structure. Here u is an *average velocity* constant, with dimension $[L] / [T]$; η is a space scale (inspired to the notation of the so-called Kolmogorov scale), with dimension $[L]$; H is the Hurst index of the independent real-valued Fractional Brownian Motions (FBM) $B_t^{H, \mathbf{k}}$, which have dimension $[T]^H$ (due to the property $\mathbb{E} \left[\left| B_t^{H, \mathbf{k}} \right|^2 \right] = t^{2H}$); the index

set \mathbf{K}_η will correspond (in the nontrivial case) to *length scales of order* η , and it is assumed to be a finite set; the divergence free vector fields $\sigma_{\mathbf{k}}(\mathbf{x})$ will be described below in the examples, and are dimensionless. The normalizing constant $C(\eta, H)$ has dimension $[T]^{1-H}$, to compensates the dimension $[T]^{H-1}$ of $\frac{dB_t^{H,\mathbf{k}}}{dt}$. Precisely, the constant $C(\eta, \tau, H)$ is given by

$$C(\eta, \tau, H) = \frac{\tau^{1-H} \sqrt{2}}{\sqrt{\Gamma(2H+1)}} \frac{1}{C_\eta}$$

where τ has the meaning of *relaxation time* of the fluid, and it is typically a small constant, with dimension $[T]$, $\Gamma(r)$ is the Gamma function and the constant $\frac{1}{C_\eta}$ is a normalizing factor for the sum over \mathbf{k} of the $\sigma_{\mathbf{k}}$, defined by (9) below. We give a precise motivation for the choice of the noise and all the constants in its definition in Appendix A.

Thanks to the factor $u\tau^{1-H}$, we keep memory of the fact that a true fluid has a finite relaxation time and a finite kinetic energy, properties that are formally lost in the model above. Indeed, the Fractional Gaussian Noise (FGN) $\frac{dB_t^{H,\mathbf{k}}}{dt}$ does not have a characteristic time-scale and has infinite variance.

Thanks to the precise normalizing factor $C(\eta, \tau, H)$, we may compare quantitatively different values of H and η (see Appendix A). The natural idea to put different models of the previous form on the same ground would be to impose that they have the same average kinetic energy; but, as we have already remarked, the FGN $\frac{dB_t^{H,\mathbf{k}}}{dt}$ has infinite variance. Hence we introduce an Ornstein-Uhlenbeck approximation

$$\mathbf{u}_\tau(\mathbf{x}, t) = \frac{u}{C_\eta} \sum_{\mathbf{k} \in \mathbf{K}_\eta} \sigma_{\mathbf{k}}(\mathbf{x}) Z_t^{\tau, H, \mathbf{k}} \quad (5)$$

where $Z_t^{\tau, H, \mathbf{k}}$ is the solution of equation

$$dZ_t^{\tau, H, \mathbf{k}} = -\frac{1}{\tau} Z_t^{\tau, H, \mathbf{k}} dt + \frac{c_H}{\tau^H} dB_t^{H, \mathbf{k}} \quad (6)$$

with $Z_0^{\tau, H, \mathbf{k}} = 0$ and c_H chosen so that $\mathbb{E} \left[\left| Z_t^{\tau, H, \mathbf{k}} \right|^2 \right] \rightarrow 1$ as $t \rightarrow \infty$ (the factor τ^H in the noise term $\frac{c_H}{\tau^H} dB_t^{H, \mathbf{k}}$ compensate the dimension of $B_t^{H, \mathbf{k}}$ to produce the adimensional quantity $Z_t^{\tau, H, \mathbf{k}}$); it is given by $c_H = \frac{\sqrt{2}}{\sqrt{\Gamma(2H+1)}}$ (see Appendix A). As shown in Lemma 6, the previous equation can be approximated by

$$Z_t^{\tau, H, \mathbf{k}} \sim \tau^{1-H} c_H dB_t^{H, \mathbf{k}} \quad (7)$$

which leads to the model above. Process (7) is more amenable to analytical treatment than (6) and therefore adopted in this work as a surrogate of the

OU process. Moreover, we consider this "normalization" an important step in view of the comparison between different forms of stochastic transport.

Concerning the smooth divergence free vector fields $\sigma_{\mathbf{k}}$, we assume that the limits

$$\langle \sigma_{\mathbf{k}} \rangle^2 := \lim_{R \rightarrow \infty} \frac{1}{R^2} \int_{[-\frac{R}{2}, \frac{R}{2}]^2} |\sigma_{\mathbf{k}}(\mathbf{x})|^2 dx \quad (8)$$

exist, and take C_{η} above given by

$$C_{\eta} = \sqrt{\sum_{\mathbf{k} \in \mathbf{K}_{\eta}} \langle \sigma_{\mathbf{k}} \rangle^2}. \quad (9)$$

2.1 Specific examples and motivation

In the choice of the two examples below we are motivated by a certain variety of turbulent flows appearing in confined plasma experiments and simulations. We will not treat realistic velocity fields emerging from such application but only paradigmatic idealizations, however inspired by such observations.

It is observed that, in the poloidal section, the electromagnetic field, which originally is perturbed at a very small scale by certain instabilities, becomes organized also in structures of vortical type having a larger coherent scale. A stochastic parametrization of them could involve FGN with Hurst parameter $H > 1/2$, to model the persistence of the perturbation (the larger a structure is, the more persistent is its transport effect). See for instance, in the review [25], Figures 9, 11, 14: sometimes the perturbations are very disordered, sometimes else they are organized in relatively parallel stripes (streamers, transport barriers). What happens to heat and matter subject to such a velocity field? Which are the turbulent transport properties?

We then consider two paradigmatic cases. The first one is simply made of constant vector fields; it is not very realistic w.r.t. such applications but it serves as a reference case. Moreover, even if so abstract, it behaves similarly to "streamers", namely coherent elongated structures. The second one is made of several disordered small-scale structures. Let us introduce the formal definitions.

The trivial case, that we call *control case*, discussed mostly for comparison, is defined by

$$\mathbf{K}_{\eta} = \{1, 2\}, \quad \sigma_1(\mathbf{x}) = (1, 0), \sigma_2(\mathbf{x}) = (0, 1).$$

We have $\langle \sigma_i \rangle^2 = 1$ for both $i = 1, 2$, hence $C_{\eta} = \sqrt{2}$,

$$C(\eta, \tau, H) = \frac{\tau^{1-H}}{\sqrt{\Gamma(2H+1)}}$$

$$\mathbf{u}(\mathbf{x}, t) = u \frac{\tau^{1-H}}{\sqrt{\Gamma(2H+1)}} \left(\frac{dB_t^{H,1}}{dt}, \frac{dB_t^{H,2}}{dt} \right).$$

We then introduce the so-called *test case*, defined by a number $\eta > 0$,

$$\begin{aligned} \mathbf{K}_\eta &= \left\{ \mathbf{k} \in \mathbb{Z}^2 : |\mathbf{k}| \in \left[\frac{1}{2\eta}, \frac{1}{\eta} \right] \right\} \\ \sigma_{\mathbf{k}}(\mathbf{x}) &= \frac{\mathbf{k}^\perp}{|\mathbf{k}|} \cos(\mathbf{k} \cdot \mathbf{x}) \quad \text{if } \mathbf{k} \in \mathbf{K}_\eta^+ \\ \sigma_{\mathbf{k}}(\mathbf{x}) &= \frac{\mathbf{k}^\perp}{|\mathbf{k}|} \sin(\mathbf{k} \cdot \mathbf{x}) \quad \text{if } \mathbf{k} \in \mathbf{K}_\eta^- \end{aligned} \quad (10)$$

where \mathbf{K}_η^+ is the set of $\mathbf{k} = (k_1, k_2) \in \mathbf{K}_\eta$ such that either $\{k_1 > 0\}$ or $\{k_1 = 0, k_2 > 0\}$, and $\mathbf{K}_\eta^- = -\mathbf{K}_\eta^+$. In this example, for each \mathbf{k} , one has

$$\langle \sigma_{\mathbf{k}} \rangle^2 = \frac{1}{2\pi} \int_0^{2\pi} \sin^2 t dt = \frac{1}{2}$$

hence

$$C_\eta = \sqrt{\frac{\text{Card}(\mathbf{K}_\eta)}{2}} \sim \frac{\sqrt{3\pi}}{2\sqrt{2\eta}} \quad (11)$$

for small η (because $\text{Card}(\mathbf{K}_\eta) \sim \pi \frac{1}{\eta^2} - \pi \frac{1}{4\eta^2} = \pi \frac{3}{4\eta^2}$).

As already said, we choose to describe the persistency of the structures by independent FGN processes $\frac{dB_t^{H,\mathbf{k}}}{dt}$ with

$$H \geq \frac{1}{2}.$$

Concerning the interpretation of the product rule $\mathbf{u} \cdot \nabla T$ and the analogous product rule in equation (13) below, if $H = \frac{1}{2}$ (case of Brownian Motion) we use Stratonovich interpretation; if $H > \frac{1}{2}$, we use Young integrals, which also are Stratonovich integrals, in a sense, if compared to Skorohod ones (see [Nualart]). In both cases, when necessary, we use the notation \circ to recall that we use Stratonovich interpretation.

2.2 Transported quantities

By solution $T(\mathbf{x}, t)$ of the transport equation above we mean, by definition, the stochastic process $T(\mathbf{x}, t)$ uniquely identified by the formula

$$T(\mathbf{X}_t^{\mathbf{x}}, t) = T_0(\mathbf{x}) \quad (12)$$

where $\mathbf{X}_t^{\mathbf{x}}$ is the solution of the equations of characteristics

$$d\mathbf{X}_t^{\mathbf{x}} = uC(\eta, \tau, H) \sum_{\mathbf{k} \in \mathbf{K}_\eta} \sigma_{\mathbf{k}}(\mathbf{X}_t^{\mathbf{x}}) \circ dB_t^{H,\mathbf{k}}, \quad \mathbf{X}_0^{\mathbf{x}} = \mathbf{x}. \quad (13)$$

The Lagrangian formulation can be proved to be equivalent to the SPDE above in many cases. Here, for simplicity, we take it as the starting point, also because we shall use numerical methods based on the Lagrangian formulation.

The key information we are interested in is how fast the information is spread, diffused, by the velocity field. Therefore the key indicator is the function

$$t \mapsto \mathbb{E} \left[|\mathbf{X}_t^0|^2 \right]. \quad (14)$$

In Appendix B we discuss the more general problem of understanding $T(\mathbf{x}, t)$, but we restrict the numerical simulations and the result to the quantity (14). Moreover, we give some theoretical a priori information on some of these quantities, that can be used to check the validity of the numerical simulations.

2.3 Main results

We here outline a synthetic description of the main results. They will be described in detail in Section 3.

As a preliminary step we simulate the process \mathbf{X}_t^0 , solution of equation (13), in the *control case*, we obviously get a FBM, as also described below in Appendix B. We use the control case to compute (14) for $H > 1/2$ and validate our numerical simulation against theory.

The main discovery of this paper is that, when we simulate the *test case*, with $H > 1/2$, after a short transient the process behaves like a Brownian Motion. The memory related to H is lost. A trace of H remains in the diffusion coefficient:

$$\sigma^2(\eta, \tau, H) \sim \frac{\mathbb{E} \left[|\mathbf{X}_t^0|^2 \right]}{t} \text{ for } t \text{ large enough.}$$

We have not found a theoretical proof of this fact until now, but the heuristic reason is relatively clear: the particle \mathbf{X}_t^0 feels at time some components of the noise more than others, and changes the most relevant components frequently, in its erratic motion. But different components have independent processes: this restores a form of independence of the increments, like for Brownian Motion. The numerical simulations of the present paper seem to indicate the validity of the following theoretical result.

Theorem 1 *Given the value of all other coefficients, choose*

$$\tau = \tau_\eta = C\eta^{\frac{1-2H}{1-H}}$$

for some constant $C > 0$. Then the process \mathbf{X}_t^0 , which depends on $\eta > 0$, converges in law to a 2-dimensional Brownian Motion in the limit as $\eta \rightarrow 0$.

Remark 2 Notice that the factor $\tau_\eta^{\frac{1}{2H}-\frac{1}{2}}\eta^{1-\frac{1}{2H}}$ in formula (15) is constant as $\eta \rightarrow 0$, under the condition of the Theorem.

Our numerical simulations indicate a Brownian behavior already for finite η , but it cannot be strictly true, since - in spite of the explanation given in Appendix C - the process "feels" the presence of all the finite number of fractional processes all the time, hence there is certainly a residual of memory, although numerically very small. In the limit when $\eta \rightarrow 0$ the number of "vortex structures" of the noise goes to infinity, the process "jumps" for one to the other and the approximate property of independent increments observed for finite η may become strict.

We do not know whether the previous theorem is true or not and hope its statement will trigger research on it. For the time being, we offer the following very partial numerical verification.

Let us introduce the quantity

$$\sigma_t^2(\eta, \tau, H) = \frac{\mathbb{E}[|\mathbf{X}_t^0|^2]}{t}, \quad \text{for } t > 0$$

and its oscillation on a generic interval $[t_0, t_1] \subset (0, \infty)$

$$\Delta(t_0, t_1, \eta, \tau, H) = \sup_{t \in [t_0, t_1]} \sigma_t^2(\eta, \tau, H) - \inf_{t \in [t_0, t_1]} \sigma_t^2(\eta, \tau, H).$$

We claim (in the numerical sense)

Claim 3 For $\tau = \tau_\eta = \eta^{\frac{1-2H}{1-H}}$, for every $[t_0, t_1] \subset (0, \infty)$,

$$\lim_{\eta \rightarrow 0} \Delta(t_0, t_1, \eta, \tau_\eta, H) = 0. \quad (15)$$

In Appendix C we add further discussion to this problem.

3 Numerical results

In this section we perform numerical simulations of transport equation (3) with advection velocity $\mathbf{u}(\mathbf{x}, t)$ given by the stochastic model (4). A Monte Carlo method is employed where particle trajectories are simulated by numerical integration of the equations of characteristics (13). Expected values and probabilities are thus approximated by appropriate ensemble averages. To illustrate the physics captured by our stochastic model we consider $H = 0.7$. A simple explicit Euler method is used in all simulations to discrete time. The converge properties of Euler's method in the range $H > 0.5$ can be found at [2].

As a preliminary step, we validate our numerical code against the theoretical predictions of the control case (see Appendix B.2). The velocity u

and the relaxation time τ_η are set to 1 and 10^{-2} , respectively. In the left panel of Fig. 1 the probability $\mathbb{P}[|x(t) - x(0)| < R]$ is computed over 10^4 realisations as a function of time (solid line) and compared with formula (18) represented by the dashed line. Evidently, for $t \gg \tau_\eta$ the theoretical prediction and the numerical result overlap. In the right panel of Fig. 1 we report $\mathbb{E}[|x(t) - x(0)|^2]$ as a function of time for the same test case. Analogously, the numerical values (solid line) match the exact formula (dashed line) for $t \gg \tau_\eta$ as predicted.

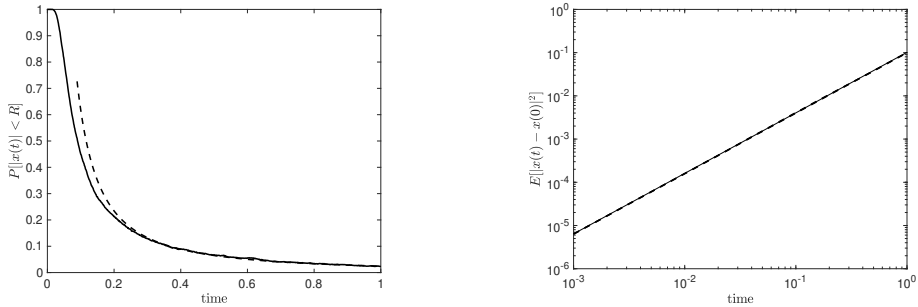


Figure 1: Probability $\mathbb{P}[|x(t) - x(0)| < R]$ (left panel) and variance $\mathbb{E}[|x(t) - x(0)|^2]$ (right panel) for the control case as a function of time. Numerical values are represented by the solid lines while the exact formulae are represented by the dashed lines.

Having validated our numerical code, we move on to simulate non-trivial vector fields $\sigma_{\mathbf{k}}$. In particular, we consider the vector field defined by (10), which represents a random perturbation concentrated at a length scale η . Having set $H = 0.7$ we expect a particle transported by such $\mathbf{u}(\mathbf{x}, t)$ to feel the “memory effect” due to correlated Brownian increments. An interesting question is then for how long this physical mechanism is maintained along a particle trajectory. To this aim we consider three values of $\eta = 2\pi/20, 2\pi/100, 2\pi/200$. Reference velocity u and relaxation time τ are set to 2 and 10^{-2} , respectively. Statistics are collected over 10^4 realisations. Fig. 2 shows the variance $\mathbb{E}[|x(t) - x(0)|^2]$ as a function of time for the simulated values of η . This numerical test clearly highlights the presence of two regimes. For small times the Fractional Brownian Noise is dominant as a slope equal to $2H$ in the variance highlights. For larger times the classical Brownian Motion prevail restoring the variance scaling to 1. Moreover, the time scale t^* of departure between the two slopes decreases with η and its value depends on the choice of parameters $C(\eta, \tau, H)$ and u . For $t \ll t^*$ the vector fields $\sigma_{\mathbf{k}}$ are approximately constant and the resulting motion is clearly an FBM. As time increases, i.e. the particle travels a distance of order η , the particle is selectively affected by independent components of the noise thus restoring Brownian Motion, as heuristically motivated in Sec.

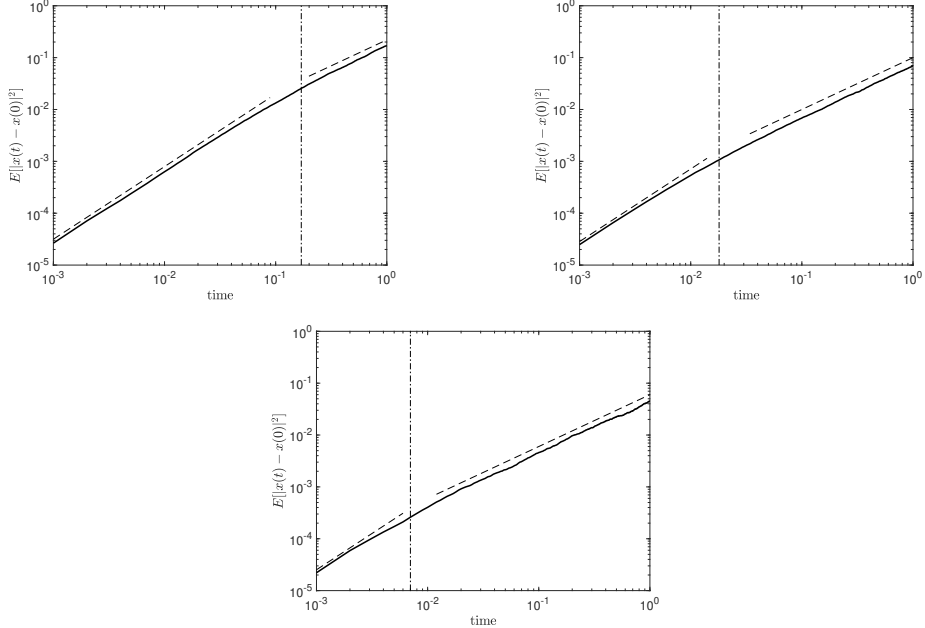


Figure 2: Variance $\mathbb{E}[|x(t) - x(0)|^2]$ for $\eta = \pi/20$ (left panel), $\eta = \pi/100$ (right panel) and $\eta = \pi/200$ (bottom panel) as a function of time. The dashed lines represents the slopes $2H$ and 1 . The dash-dotted vertical line represents $t = t^*$.

2.3. In the plots of Fig. 2) t^* (vertical lines in Fig. 2) is set to be the time at which the particle has travelled approximately a distance of $\eta/2$.

The standard deviation of the Brownian Motion established in the region for $t \gg t^*$, called σ_H , can be estimated by a diffusive approximation of the fractional Brownian Motion as detailed in Appendix C. In Fig. 3 σ_H computed from numerical simulation is shown as function of η (dots) and compared against expression (20) (solid line). A good agreement of the theoretical prediction with the numerical results is found. The free parameter λ computed using a least-squares method is approximately 0.47. The latter is, however, not a universal constant but rather it has been found dependent on $\sigma_{\mathbf{k}}$. To show this behaviour we generalise (10) to

$$\begin{aligned} \sigma_{\mathbf{k}}(\mathbf{x}) &= \frac{\mathbf{k}^\perp}{|\mathbf{k}|} g(\cos(\mathbf{k} \cdot \mathbf{x})) & \text{if } \mathbf{k} \in \mathbf{K}_\eta^+ \\ \sigma_{\mathbf{k}}(\mathbf{x}) &= \frac{\mathbf{k}^\perp}{|\mathbf{k}|} g(\sin(\mathbf{k} \cdot \mathbf{x})) & \text{if } \mathbf{k} \in \mathbf{K}_\eta^- \end{aligned} \quad (16)$$

where

$$g(r) = \tanh(Mr),$$

is an approximation of the sign function with smoothness controlled by the

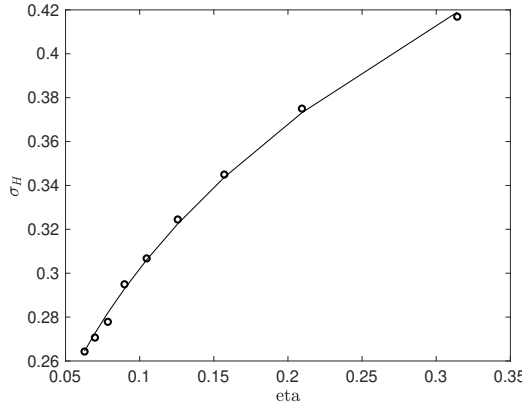


Figure 3: Standard deviation σ_H as a function of η computed numerically (dots) and analytically (solid line) using (20).

parameter M . By repeating the above procedure we find $\lambda \approx 0.41$ for $M = 10$. We thus conclude that there exists indeed a constant λ , but it is not universal.

A concise way to state our results is formulated by Claim (15). While proving this statement is challenging, we here limit ourselves to simulate the oscillation $\Delta(t_0, t_1, \eta, \tau, H)$ for decreasing values of η . The findings, re-

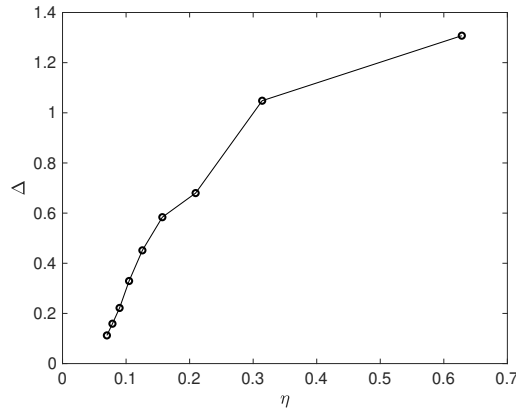


Figure 4: Oscillation $\Delta(t_0, t_1, \eta, \tau, H)$ as a function of η computed numerically.

ported in Fig. 4, support our claim with Δ approaching zero as η decreases. We remark, however, that the limit $\eta \rightarrow 0$ is computationally not feasible. To smaller η there correspond larger radius in spectral space therefore increasing the terms to be computed, at each time step, in the expression of $\sigma_{\mathbf{k}}$. Furthermore, the velocity components of smaller length-scale η have

larger gradients, which require a finer time step to be properly resolved. This, in practice, has limited the numerical investigation conducted here to $\eta \approx 7 \cdot 10^{-2}$. Nevertheless, the trend is indeed in agreement with our predictions.

As a final and more involved illustration of our stochastic model we consider the evolution of an ensemble of $N = 10^3$ particles. The underlying vector field is again given by (10) where we set $\eta = 2\pi/20$. The particles are released at $t = 0$ according to a uniform random distribution in a circle of radius $R = \eta/8$ centred at the origin. A number of 10^3 realisations is simulated and the variance $\text{VAR}_N(t) = \frac{1}{N} \sum_{i=1}^N \mathbb{E}[|\mathbf{x}_i(t)|^2]$ is computed over time. The qualitative behaviour of this swarm of particles is shown in Fig. 5 where the simulated particle positions are drawn at different times. For $t \ll t^*$ (top-right panel) the particles are pushed around the origin by an approximately spatially uniform velocity, thus maintaining an almost circular shape. For times of order t^* (mid-left and mid-right panel) particles tend to agglomerate in regions where the vector field components $\sigma_{\mathbf{k}}$ sum to zero, which are characterised by a typical length scale of order η . Finally, for $t \gg t^*$ (bottom-right and bottom-left panel) the particles are picked up by different and independent waves composing the noise and thus loosing all structures inserted in the initial conditions.

Fig. 6 shows $\text{VAR}_N(t)$ for $H = 0.7$ (solid line) and $H = 0.5$ (dash-dotted line). The Hurst exponent does not appear to have a significant influence for $t \ll t^*$ where the collective behaviour of the particles is dominated by the particular choice of vector field components $\sigma_{\mathbf{k}}$. As time becomes much larger than t^* a Brownian Motion dispersion is recovered. However, to a larger H there corresponds a larger variance as suggested by Remark 6. of Appendix C.

4 Conclusions

We have investigated the dispersion of particles transported by a stochastic vector field driven by fractional gaussian processes at different scales. We found the existence of two regimes: at small times compared to those taken by a particle to travel a distance of order η , the motion is governed by the fractional gaussian process of the single vector field components. As the particle travels distances larger than η , a standard Brownian Motion is recovered. This behaviour is indicated by the double slope in the variance found in the numerical simulations, ranging from $H > 1/2$ in the first regime to $H = 1/2$ in the second regime. We derived, by a diffusion approximation, an expression for the standard deviation of the Brownian Motion established in the second regime and verified the formula against numerical predictions. A good agreement was found up to an arbitrary constant λ .

We then postulated Theorem 1 where converges in law to a 2-dimensional

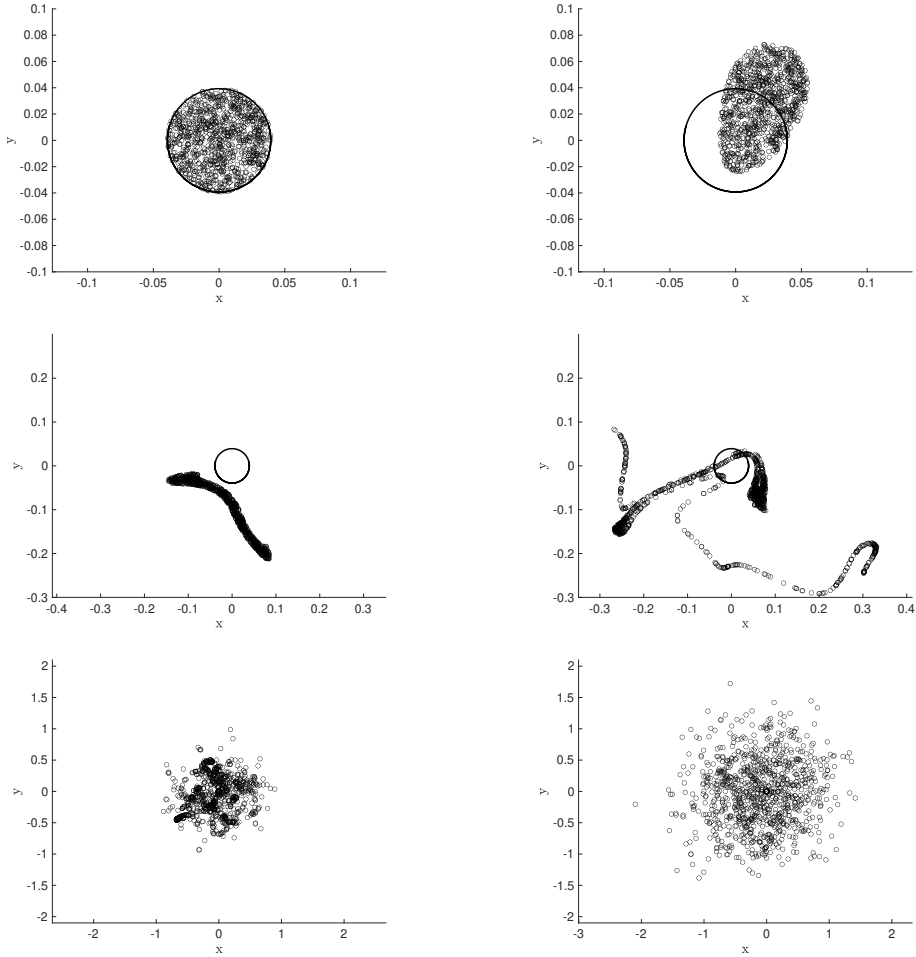


Figure 5: Particle positions at $t = 0$ (top-left panel), $t = t^*/10$ (top-right panel), $t = t^*$ (mid-left panel), $t = 4t^*$ (mid-right panel), $t = 10t^*$ (bottom-left panel) and $t = 25t^*$ (bottom-right panel). The circle $r = \eta/8$ is depicted by solid line in all figures as point of reference.

Brownian is expected in the limit $\eta \rightarrow 0$. No attempt to prove this theorem was made in this work, but rather we empirically tested its validity through numerical simulations. Our findings, even though computationally limited to a finite η , are consistent to the statement of Theorem 1. We hope that this work will spark interest in the scientific community and serve as a base ground to build upon further studies on Fractional Brownian Motion.

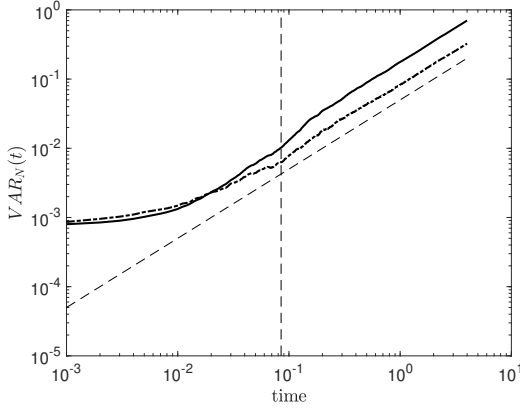


Figure 6: Particles variance $VAR_N(t)$ as a function of time for $H = 0.7$ (solid line) and $H = 0.5$ (dash-dotted line). Slope 1 is represented by the inclined dashed line while $t = t^*$ is represented by the vertical dashed line.

A Model scaling

Consider the velocity field $\mathbf{u}_\tau(\mathbf{x}, t)$ given by equation (5), where $Z_t^{\tau, H, \mathbf{k}}$ is given by (6) and $B_t^{H, \mathbf{k}}$ are independent FBM's.

Remark 4 In law, $Z_t^{\tau, H, \mathbf{k}} = \theta_{t/\tau}^{H, \mathbf{k}}$ where $\theta_t^{H, \mathbf{k}}$ satisfies

$$d\theta_t^{H, \mathbf{k}} = -\theta_t^{H, \mathbf{k}} dt + \frac{\sqrt{2}}{\sqrt{\Gamma(2H+1)}} dB_t^{H, \mathbf{k}}.$$

The proof is based on the fact that

$$\frac{1}{\tau} \frac{dB_t^{H, \mathbf{k}}}{dt} \Big|_{\frac{t}{\tau}} = \frac{d}{dt} B_{t/\tau}^{H, \mathbf{k}} = \tau^{-H} \frac{d}{dt} \tau^H B_{t/\tau}^{H, \mathbf{k}} = \tau^{-H} \frac{d}{dt} \tilde{B}_t^{H, \mathbf{k}}$$

where $\tilde{B}_t^{H, \mathbf{k}}$ is another FBM, since $\tau^H B_{t/\tau}^{H, \mathbf{k}} \stackrel{\mathcal{L}}{=} \tilde{B}_t^{H, \mathbf{k}}$.

We have:

Lemma 5 $\mathbb{E} \left[Z_t^{\tau, H, \mathbf{k}} \right] = 0$,

$$\lim_{t \rightarrow \infty} \mathbb{E} \left[\left(Z_t^{\tau, H, \mathbf{k}} \right)^2 \right] = 1 \quad (17)$$

Proof. We have

$$Z_t^{\tau, H, \mathbf{k}} = \int_0^t e^{-\frac{t-s}{\tau}} \frac{\sqrt{2}}{\sqrt{\Gamma(2H+1)} \tau^H} dB_s^{H, \mathbf{k}}.$$

From [2], Chapter 5, Section 1, we have

$$\begin{aligned}\mathbb{E} \left[\left(\int_0^t e^{-\frac{t-s}{\tau}} dB_s^{H,\mathbf{k}} \right)^2 \right] &= H(2H-1) \int_0^t \int_0^t e^{-\frac{t-s}{\tau}} e^{-\frac{t-r}{\tau}} |s-r|^{2H-2} ds dr \\ &= H(2H-1) \int_0^t \int_0^t e^{-\frac{s}{\tau}} e^{-\frac{r}{\tau}} |s-r|^{2H-2} ds dr.\end{aligned}$$

Therefore

$$\begin{aligned}\lim_{t \rightarrow \infty} \mathbb{E} \left[\left(Z_t^{\tau,H,\mathbf{k}} \right)^2 \right] &= \frac{2}{\Gamma(2H+1) \tau^{2H}} H(2H-1) \int_0^\infty \int_0^\infty e^{-\frac{s}{\tau}} e^{-\frac{r}{\tau}} |s-r|^{2H-2} ds dr \\ &= \frac{2H(2H-1)}{\Gamma(2H+1)} \int_0^\infty \int_0^\infty e^{-s'} e^{-r'} |s'-r'|^{2H-2} ds' dr' \\ &= 1\end{aligned}$$

because

$$\begin{aligned}&\int_0^\infty \int_0^\infty e^{-s} e^{-r} |s-r|^{2H-2} ds dr \\ &= 2 \int_0^\infty e^{-s} \left(\int_0^s e^{-r} |s-r|^{2H-2} dr \right) ds \\ &= 2 \int_0^\infty e^{-2s} \left(\int_0^s e^r r^{2H-2} dr \right) ds \\ &= 2 \left[-\frac{1}{2} e^{-2s} \int_0^s e^r r^{2H-2} dr \right]_{s=0}^{s=\infty} + 2 \int_0^\infty \frac{1}{2} e^{-2s} e^s s^{2H-2} ds \\ &= \int_0^\infty e^{-s} s^{2H-2} ds = \Gamma(2H-1) = \frac{\Gamma(2H+1)}{2H(2H-1)}\end{aligned}$$

recalling that $\Gamma(z+1) = \int_0^\infty e^{-s} s^z ds$ and $\Gamma(z+1) = z\Gamma(z)$. \blacksquare

From the result of Lemma 5 and the independence,

$$\mathbb{E} \left[|\mathbf{u}_\tau(\mathbf{x}, t)|^2 \right] = \frac{u^2}{C_\eta^2} \sum_{\mathbf{k} \in \mathbf{K}_\eta} |\sigma_{\mathbf{k}}(\mathbf{x})|^2.$$

Hence (recall (8)-(9)) the limit

$$\langle \mathbf{u}_\tau \rangle^2 := \lim_{R \rightarrow \infty} \frac{1}{R^2} \int_{[-\frac{R}{2}, \frac{R}{2}]^2} \mathbb{E} \left[|\mathbf{u}_\tau(\mathbf{x}, t)|^2 \right] dx$$

exists and is given by

$$\langle \mathbf{u}_\tau \rangle^2 = u^2.$$

This is the motivation for calling u^2 the mean square turbulent velocity (or turbulent kinetic energy, multiplied by 2). Moreover, the velocity fields $\mathbf{u}_\tau(\cdot, t)$ are *instantaneously* on the same ground with respect to the parameters η, τ, H , namely at a given time they have the same average intensity.

Since

$$\tau dZ_t^{\tau, H, \mathbf{k}} = -Z_t^{\tau, H, \mathbf{k}} dt + \tau^{1-H} \frac{\sqrt{2}}{\sqrt{\Gamma(2H+1)}} dB_t^{H, \mathbf{k}}$$

we may conjecture that

$$Z_t^{\tau, H, \mathbf{k}} dt \sim \tau^{1-H} \frac{\sqrt{2}}{\sqrt{\Gamma(2H+1)}} dB_t^{H, \mathbf{k}}.$$

This fact has a rigorous formulation as shown in the next lemma. On its basis, we replace the velocity field $\mathbf{u}_\tau(\mathbf{x}, t)$ above by

$$\mathbf{u}(\mathbf{x}, t) = \frac{u\tau^{1-H}\sqrt{2}}{\sqrt{\Gamma(2H+1)}C_\eta} \sum_{\mathbf{k} \in \mathbf{K}_\eta} \sigma_\mathbf{k}(\mathbf{x}) \frac{dB_t^{H, \mathbf{k}}}{dt}.$$

Lemma 6

$$\mathbb{E} \left[\left(\int_0^t Z_s^{\tau, H, \mathbf{k}} ds - \tau^{1-H} \frac{\sqrt{2}}{\sqrt{\Gamma(2H+1)}} B_t^{H, \mathbf{k}} \right)^2 \right] \leq \tau^{2-2H}.$$

Proof. As a preliminary remark, we notice that one can use Fubini theorem also for the Wiener integrals with respect to fractional Brownian motion, thanks to the reformulation

$$\int_0^t e^{-\frac{(t-s)}{\tau}} dB_s^{H, \mathbf{k}} = -\frac{1}{\tau} \int_0^t e^{-\frac{(t-s)}{\tau}} B_s^{H, \mathbf{k}} ds + B_t^{H, \mathbf{k}}$$

and the application of Fubini theorem to the classical integral on the right-hand-side of this identity. Based on this preliminary fact, we have

$$\begin{aligned} \int_0^t Z_s^{\tau, H, \mathbf{k}} ds &= \frac{\sqrt{2}}{\sqrt{\Gamma(2H+1)}\tau^H} \int_0^t \left(\int_0^s e^{-\frac{(s-r)}{\tau}} dB_r^{H, \mathbf{k}} \right) ds \\ &= \tau^{1-H} \frac{\sqrt{2}}{\sqrt{\Gamma(2H+1)}} \int_0^t \left(\int_r^t \frac{1}{\tau} e^{-\frac{(s-r)}{\tau}} ds \right) dB_r^{H, \mathbf{k}} \\ &= \tau^{1-H} \frac{\sqrt{2}}{\sqrt{\Gamma(2H+1)}} B_t^{H, \mathbf{k}} + R_t^{H, \mathbf{k}} \end{aligned}$$

having used $\int_r^t \frac{1}{\tau} e^{-\frac{(s-r)}{\tau}} ds = 1 - e^{-\frac{(t-r)}{\tau}}$, where we set

$$R_t^{H, \mathbf{k}} = \tau^{1-H} \frac{\sqrt{2}}{\sqrt{\Gamma(2H+1)}} \int_0^t e^{-\frac{(t-r)}{\tau}} dB_r^{H, \mathbf{k}}.$$

Then it is sufficient to prove that

$$\mathbb{E} \left[(R_t^{H, \mathbf{k}})^2 \right] \leq \tau^{2-2H}.$$

But this follows immediately from the result of the previous lemma. \blacksquare

B On formula (12)

In this appendix we discuss the formula (12). If $\phi : \mathbb{R}^2 \rightarrow \mathbb{R}$ is a measurable compact support test function, then

$$\langle T(t), \phi \rangle = \int \phi(\mathbf{y}) T(\mathbf{y}, t) d^2y = \int \phi(\mathbf{X}_t^{\mathbf{x}}) T(\mathbf{X}_t^{\mathbf{x}}, t) d^2x = \int \phi(\mathbf{X}_t^{\mathbf{x}}) T_0(\mathbf{x}) d^2x$$

where the intermediate identity, based on the change of variable $\mathbf{y} = \mathbf{X}_t^{\mathbf{x}}$, is due to the fact that the determinant of the Jacobian of $\mathbf{x} \rightarrow \mathbf{X}_t^{\mathbf{x}}$ solves an equation with the trace of the derivative of the $\sigma_{\mathbf{k}}(\mathbf{x})$, which is the divergence of $\sigma_{\mathbf{k}}(\mathbf{x})$, hence equal to zero; therefore the Jacobian determinant is equal to one.

In case one is interested in single realizations of $\langle T(t), \phi \rangle$, a numerical method is the following one: generate a sample of N points \mathbf{x}_i , $i = 1, \dots, N$, distributed according to the density $T_0(\mathbf{x})$, hence compute

$$\langle T(t), \phi \rangle \sim \frac{1}{N} \sum_{i=1}^N \phi(\mathbf{X}_t^{\mathbf{x}_i}).$$

However, here we mean that we use the same noise realizations for each one of the points \mathbf{x}_i .

In this paper we want to investigate a number of quantities, depending on the Hurst exponent H and the set \mathbf{K}_η (and ϕ):

1. the function $t \mapsto \mathbb{E} [|\mathbf{X}_t^0|^2]$
2. the mean value $t \mapsto m_t^\phi = \mathbb{E} [\langle T(t), \phi \rangle]$
3. the variance $t \mapsto \mathbb{E} \left[(\langle T(t), \phi \rangle - m_t^\phi)^2 \right]$.

B.1 Particular choice of T_0 and ϕ

Let us make the following special choices:

$$T_0 = \delta_0$$

namely the weak limit of densities of the form $T_0^\epsilon(\mathbf{x}) = \epsilon^{-2} \theta(\epsilon^{-1} \mathbf{x})$ with suitable pdf θ , and

$$\phi = 1_{B(\mathbf{0}, R)}$$

the indicator function of the ball $B(\mathbf{0}, R)$. We expect, in the average, a decrease of $\langle T(t), \phi \rangle$.

In this case, using the formula $\langle T(t), \phi \rangle = \int \phi(\mathbf{X}_t^{\mathbf{x}}) T_0(\mathbf{x}) d^2x$ and the approximation of $T_0 = \delta_0$ by T_0^ϵ , we get

$$\langle T(t), \phi \rangle = \phi(\mathbf{X}_t^0) = \begin{cases} 1 & \text{if } |\mathbf{X}_t^0| < R \\ 0 & \text{if } |\mathbf{X}_t^0| \geq R \end{cases}$$

and therefore

$$\begin{aligned}\mathbb{E} [\langle T(t), \phi \rangle] &= \mathbb{P} (|\mathbf{X}_t^0| < R) \\ \mathbb{E} \left[\left(\langle T(t), \phi \rangle - m_t^\phi \right)^2 \right] &= \mathbb{E} [\phi(\mathbf{X}_t^0)^2] - \mathbb{P} (|\mathbf{X}_t^0| < R)^2 = \mathbb{P} (|\mathbf{X}_t^0| < R) - \mathbb{P} (|\mathbf{X}_t^0| < R)^2 \\ (\text{because } \phi(\mathbf{X}_t^0)^2 &= \phi(\mathbf{X}_t^0)) \\ &= \mathbb{P} (|\mathbf{X}_t^0| < R) (1 - \mathbb{P} (|\mathbf{X}_t^0| < R)).\end{aligned}$$

Therefore, the key quantities in this example of T_0 and ϕ are:

1. the function $t \mapsto \mathbb{E} [|\mathbf{X}_t^0|^2]$
2. the function $t \mapsto \mathbb{P} (|\mathbf{X}_t^0| < R)$.

B.2 Exact formulae in the control case

In the control case $\mathbf{K}_\eta = \{1, 2\}$, equation (13) read

$$d\mathbf{X}_t^0 = u \frac{\tau_\eta^{1-H}}{\sqrt{\Gamma(2H+1)}} d(B_t^{H,1}, B_t^{H,2})$$

namely

$$\mathbf{X}_t^0 = u \frac{\tau_\eta^{1-H}}{\sqrt{\Gamma(2H+1)}} (B_t^{H,1}, B_t^{H,2}).$$

We have

$$\mathbb{E} [|\mathbf{X}_t^0|^2] = \frac{2}{\Gamma(2H+1)} u^2 \tau_\eta^{2-2H} t^{2H} = \frac{2}{\Gamma(2H+1)} u^2 \tau_\eta^2 \left(\frac{t}{\tau_\eta} \right)^{2H}.$$

In order to compute $\mathbb{P} (|\mathbf{X}_t^0| < R)$, denote by $\mathbf{Z} = (Z_1, Z_2)$ a standard normal vector and notice that $(B_t^{H,1}, B_t^{H,2}) = t^H \mathbf{Z}$, hence $\mathbf{X}_t^0 = \frac{u \tau_\eta^{1-H}}{\sqrt{\Gamma(2H+1)}} t^H \mathbf{Z}$. Therefore

$$\begin{aligned}\mathbb{P} (|\mathbf{X}_t^0| < R) &= \mathbb{P} (|\mathbf{Z}| < \sqrt{\Gamma(2H+1)} u^{-1} \tau_\eta^{H-1} t^{-H} R) \\ &= \mathbb{P} (Z_1^2 + Z_2^2 < \Gamma(2H+1) u^{-2} \tau_\eta^{2H-2} t^{-2H} R^2) \\ &= \mathbb{P} (Y < \Gamma(2H+1) u^{-2} \tau_\eta^{2H-2} t^{-2H} R^2)\end{aligned}$$

where Y has a Chi-squared distribution with two degrees of freedom, namely with density

$$f_{Y,2}(y) = \frac{e^{-y/2}}{2} 1_{\{y \geq 0\}}.$$

For large t we have a small value of $\epsilon = \Gamma(2H+1) u^{-2} \tau_\eta^{2H-2} t^{-2H} R^2$, hence

$$\mathbb{P} (Y < \epsilon) \sim f_{Y,2}(0) \epsilon = \frac{\epsilon}{2}$$

namely

$$\mathbb{P}(|\mathbf{X}_t^0| < R) \sim \frac{\Gamma(2H+1)}{2} u^{-2} \tau_\eta^{2H-2} t^{-2H} R^2 = \frac{\Gamma(2H+1)}{2} \frac{R^2}{u^2 \tau_\eta^2} \left(\frac{t}{\tau_\eta}\right)^{-2H} \quad (18)$$

Notice that dimensional analysis is correct. It follows, for large t ,

$$m_t^\phi = \mathbb{E}[\langle T(t), \phi \rangle] \sim \frac{\Gamma(2H+1)}{2} \frac{R^2}{u^2 \tau_\eta^2} \left(\frac{t}{\tau_\eta}\right)^{-2H}$$

and

$$\mathbb{E} \left[(\langle T(t), \phi \rangle - m_t^\phi)^2 \right] \sim \frac{\Gamma(2H+1)}{2} \frac{R^2}{u^2 \tau_\eta^2} \left(\frac{t}{\tau_\eta}\right)^{-2H} \quad (19)$$

(since $1 - \mathbb{P}(|\mathbf{X}_t^0| < R) \rightarrow 0$).

C Diffusion constant of the approximate Brownian Motion

The main result of this paper is the fact that, in spite of the memory of the processes involved, the behavior of a tracer is similar to a Brownian Motion when the spatial structure of the fluid velocity field is complex enough. A natural question is whether we can give a formula for the diffusion constant of the approximate Brownian Motion. In this appendix we conjecture a formula for this diffusion constant. The procedure to obtain it also clarifies the intuition behind the fact itself of a Brownian behavior.

Recall that the tracer dynamics, starting from zero, is defined by equation (13)

$$\mathbf{X}_t = uC(\eta, \tau, H) \sum_{\mathbf{k} \in \mathbf{K}_\eta} \int_0^t \sigma_{\mathbf{k}}(\mathbf{X}_s) \circ dB_s^{H, \mathbf{k}}.$$

Over a very short time interval $[t, t + t_\eta]$, the displacement can be approximated by

$$\mathbf{X}_{t+t_\eta} - \mathbf{X}_t \sim uC(\eta, \tau, H) \sum_{\mathbf{k} \in \mathbf{K}_\eta} \sigma_{\mathbf{k}}(\mathbf{X}_t) \left(B_{t+t_\eta}^{H, \mathbf{k}} - B_t^{H, \mathbf{k}} \right)$$

(for $H = 1/2$ we should consider the Stratonovich approximation but one can show that it is not essential for the final result; we omit this point). We perform further the following rough approximation (inspired by the computations of Appendix A)

$$\begin{aligned} |\mathbf{X}_{t+t_\eta} - \mathbf{X}_t| &\sim uC(\eta, \tau, H) \sqrt{\frac{\text{Card}(\mathbf{K}_\eta)}{2}} t^H \\ &= u \frac{\sqrt{2} \tau^{1-H}}{\sqrt{\Gamma(2H+1)}} t^H. \end{aligned}$$

We want to discover that, approximately

$$\mathbf{X}_t \sim \sigma_H \mathbf{W}_t$$

where \mathbf{W}_t is a 2d Brownian Motion. In particular, we want an estimate of σ_H . The intuition is that, in an average time t_η , the tracer jumps from a Fourier component to the other (we mean that the tracer is influenced mostly by a certain Fourier component, for a time of order t_η , then mostly by another one). The increments

$$\mathbf{X}_{t_\eta}, \mathbf{X}_{2t_\eta} - \mathbf{X}_{t_\eta}, \mathbf{X}_{3t_\eta} - \mathbf{X}_{2t_\eta}, \dots$$

will be approximately independent, since the various Fourier components are affected by independent processes. Moreover, each increment has a length $|\mathbf{X}_{(i+1)t_\eta} - \mathbf{X}_{it_\eta}|$ or order $\lambda\eta$, for a certain $\lambda > 0$. Indeed, these increments are the displacements when the tracer is affected by a certain Fourier component, before jumping on another one, but the typical "distance" to travel in order to jump from one to the other is of the order of the wave-length of the sinusoidal components of the noise, possibly reduced by a factor λ (the intuition is that the tracer is on the "top" of a cosine function, where the function takes approximately the value ± 1 ; moving a little bit, just a portion of the wave-length η , it will be no more on the top of that cosine component, but more near the top of another component).

Summarizing, at time steps t_η , we have a random walk with displacements of size $\lambda\eta$. After N time steps, the variance of the position is of order $N(\lambda\eta)^2$. In other words, at time Nt_η the square-average distance from the origin is $N(\lambda\eta)^2$. Which should be also equal to $\sigma_H^2 N t_\eta$, hence

$$\sigma_H \sim \frac{\lambda\eta}{\sqrt{t_\eta}}.$$

But we have established above that

$$\lambda\eta \sim u \frac{\sqrt{2}\tau^{1-H}}{\sqrt{\Gamma(2H+1)}} t_\eta^H.$$

Hence

$$t_\eta \sim \left(\frac{\lambda\eta \sqrt{\Gamma(2H+1)}}{\sqrt{2}\tau^{1-H} u} \right)^{1/H}$$

and finally

$$\sigma_H \sim \left(\frac{2}{\Gamma(2H+1)} \right)^{\frac{1}{4H}} u^{\frac{1}{2H}} \tau_{\eta}^{\frac{1}{2H}-\frac{1}{2}} \lambda^{1-\frac{1}{2H}} \eta^{1-\frac{1}{2H}}. \quad (20)$$

We have not found an argument to predict the coefficient λ , but we can show numerically that there exists a value providing a good fit between this formula and numerical experiments.

Remark 7 Call $K = u_{\eta}^{\frac{1}{2H}}$ the Kubo number. Recall from Appendix B that, for the Brownian Motion, $\sigma_{MB} \sim \sqrt{2}u_{\eta}\tau_{\eta}^{\frac{1}{2}}$. Hence

$$\sigma_H \sim \frac{1}{\sqrt{2}} \left(\frac{2}{\Gamma(2H+1)} \right)^{\frac{1}{4H}} \frac{\sigma_{MB}}{K^{1-\frac{1}{2H}}}$$

Therefore $\sigma_H \gg \sigma_{MB}$ if $K \ll 1$.

Acknowledgements

This research has been funded by the European Union, ERC NoisyFluid, No. 101053472.

References

- [1] Benoit B Mandelbrot and John W Van Ness. Fractional brownian motions, fractional noises and applications. *SIAM review*, 10(4):422–437, 1968.
- [2] David Nualart. *The Malliavin calculus and related topics*, volume 1995. Springer, 2006.
- [3] I Kruk and F Russo. Skorohod calculus and paley-wiener integrals for covariance singular processes (2010). arxiv.
- [4] Franco Flandoli and Francesco Russo. Reduced dissipation effect in stochastic transport by gaussian noise with regularity greater than 1/2. *arXiv preprint arXiv:2305.19293*, 2023.
- [5] Gabriel B Apolinário, Geoffrey Beck, Laurent Chevillard, Isabelle Gallagher, and Ricardo Grande. A linear stochastic model of turbulent cascades and fractional fields. *arXiv preprint arXiv:2301.00780*, 2023.
- [6] Gabriel B Apolinário, Laurent Chevillard, and Jean-Christophe Mourrat. Dynamical fractional and multifractal fields. *Journal of Statistical Physics*, 186(1):15, 2022.
- [7] Laurent Chevillard, Marc Lagoin, and Stephane G Roux. Multifractal fractional ornstein-uhlenbeck processes. *arXiv preprint arXiv:2011.09503*, 2020.
- [8] Albert Fannjiang and Tomasz Komorowski. Fractional brownian motions and enhanced diffusion in a unidirectional wave-like turbulence. *Journal of Statistical Physics*, 100:1071–1095, 2000.

- [9] Albert Fannjiang and Tomasz Komorowski. Fractional brownian motions in a limit of turbulent transport. *Annals of Applied Probability*, pages 1100–1120, 2000.
- [10] Albert Fannjiang and Tomasz Komorowski. Frozen path approximation for turbulent diffusion and fractional brownian motion in random flows. *SIAM Journal on Applied Mathematics*, 63(6):2042–2062, 2003.
- [11] Tomasz Komorowski, Alexei Novikov, and Lenya Ryzhik. Homogenization driven by a fractional brownian motion: the shear layer case. *Multiscale Modeling & Simulation*, 12(2):440–457, 2014.
- [12] Alessio Squarcini, Enzo Marinari, and Gleb Oshanin. Passive advection of fractional brownian motion by random layered flows. *New Journal of Physics*, 22(5):053052, 2020.
- [13] Lucio Galeati. On the convergence of stochastic transport equations to a deterministic parabolic one. *Stochastics and Partial Differential Equations: Analysis and Computations*, 8(4):833–868, 2020.
- [14] Franco Flandoli, Eliseo Luongo, et al. *Stochastic partial differential equations in fluid mechanics*, volume 2330. Springer, 2023.
- [15] Dejun Luo. Enhanced dissipation for stochastic navier–stokes equations with transport noise. *Journal of Dynamics and Differential Equations*, 37(1):859–894, 2025.
- [16] Bertrand Chapron, Dan Crisan, Darryl Holm, Etienne Mémin, and Anna Radomska. Stochastic transport in upper ocean dynamics. stuod 2021 workshop, london, uk, september 20–23. 2023.
- [17] Dan Crisan, Darryl D Holm, James-Michael Leahy, and Torstein Nilssen. Solution properties of the incompressible euler system with rough path advection. *Journal of Functional Analysis*, 283(9):109632, 2022.
- [18] Dan Crisan, Darryl D Holm, James-Michael Leahy, and Torstein Nilssen. Variational principles for fluid dynamics on rough paths. *arXiv preprint arXiv:2004.07829*, 2020.
- [19] Sagy R Ephrati, Paolo Cifani, Erwin Luesink, and Bernard J Geurts. Data-driven stochastic lie transport modeling of the 2d euler equations. *Journal of Advances in Modeling Earth Systems*, 15(1):e2022MS003268, 2023.
- [20] Darryl D Holm. Variational principles for stochastic fluid dynamics. *Proceedings of the Royal Society A: Mathematical, Physical and Engineering Sciences*, 471(2176):20140963, 2015.

- [21] Darryl D Holm, Erwin Luesink, and Wei Pan. Stochastic mesoscale circulation dynamics in the thermal ocean. *Physics of Fluids*, 33(4), 2021.
- [22] Etienne Mémin. Fluid flow dynamics under location uncertainty. *Geophysical & Astrophysical Fluid Dynamics*, 108(2):119–146, 2014.
- [23] Valentin Resseguier, Etienne Mémin, and Bertrand Chapron. Geophysical flows under location uncertainty, part i random transport and general models. *Geophysical & Astrophysical Fluid Dynamics*, 111(3):149–176, 2017.
- [24] Andrew J Majda and Peter R Kramer. Simplified models for turbulent diffusion: theory, numerical modelling, and physical phenomena. *Physics reports*, 314(4-5):237–574, 1999.
- [25] Xavier Garbet, Yasuhiro Idomura, Laurent Villard, and TH Watanabe. Gyrokinetic simulations of turbulent transport. *Nuclear Fusion*, 50(4):043002, 2010.